Competition between simple and complex contagion on temporal networks

Elsa Andres [1], Romualdo Pastor-Satorras [2], Michele Starnini [3,4] and Márton Karsai [1,5,*]

[1]Department of Network and Data Science, Central European University, Vienna 1100, Austria
[2]Departament de Física, Universitat Politècnica de Catalunya, Campus Nord B4, Barcelona 08034, Spain
[3]Department of Engineering, Universitat Pompeu Fabra, Barcelona 08018, Spain
[4]CENTAI, Torino 10138, Italy
[5]National Laboratory of Health Security, HUN-REN Alfréd Rényi Institute of Mathematics, Budapest 1053, Hungary

(Received 2 December 2024; accepted 16 July 2025; published 22 October 2025)

Behavioral adoptions of individuals are influenced by their peers in different ways. While in some cases an individual may change behavior after a single incoming influence, in other cases multiple cumulated attempts of social influence are necessary for the same outcome. These two mechanisms, known as simple and complex contagion, often occur together in social contagion phenomena, yet their distinguishability based on the observable contagion dynamics is challenging. In this paper we define a social contagion model evolving on temporal networks where individuals can switch between contagion mechanisms. We explore three spreading scenarios: predominated by simple or complex contagion, or where the dominant mechanism changes during the unfolding process. We propose analytical and numerical methods relying on global spreading observables to identify which of these three scenarios characterizes a social spreading outbreak. This work offers insights into social contagion dynamics on temporal networks, without assuming prior knowledge about the contagion mechanism driving the adoptions of individuals.

DOI: 10.1103/2l6j-46rh

I. INTRODUCTION

Our personal decisions—buying a product, following a trend, or adopting a hobby—are shaped not only by our own preferences but also by the influence of others [1–4]. Social influence, coming from our peers, commonly biases our choices to make us align with a larger group, who has already adapted a given behavior [5]. This phenomenon, known as social contagion [1], leads to widespread patterns of adoption across populations connected by a social network. While it has long been understood that interpersonal influence affects mass adoption [6,7], the detection of the social contagion mechanisms dominating spreading outbreak remain unclear. At the egocentric network level, according to the social brain hypothesis [8], the strength of peer influence may vary among acquaintances depending on their intimacy level [9]. This heterogeneity in influence makes it difficult to decide if a single attempt of social influence or, alternatively, repeated social stimuli, driven by reinforcement mechanisms, plays a role in the adoption of a person [10–12].

Multiple social contagion mechanisms have been identified to model the diversity of observed contagion patterns [1]. These are often defined as binary-state processes, where individuals (or nodes) move from a susceptible to an infected state due to interactions with infected others [2,13]. Simple contagion models, like the susceptible-infected (SI) dynamics [14,15], assume that a single interaction could be enough to trigger transmission, leading to smooth initial growth of spreading [16,17]. In contrast, complex contagion models [18] require multiple exposures to reach a cognitive threshold of accumulated influence before adoption occurs [10,11]. This type of mechanism accounts for rapid cascading spreading dynamics, commonly seen in the case of highly popular products or memes [19].

Contagion models often assume that social networks encode the structure that communicates influence between connected peers [19,20]. Several topological properties, such as the egocentric network size (degree) [20–22], triadic closure (clustering) [23], peerwise strength of influence (link weights) [9,24–26], or multilayer structure [27,28], play important roles in the spreading process. On the other hand, the time-varying nature of social interactions is less studied in this context, while it heavily influences the contagion dynamics, as it determines the time-respecting paths along which information or influence can be disseminated. The lifetime of links [29], the frequency of interactions [30,31], the limited waiting times of processes at nodes [32], the causally related adjacent events [33], the memory length of influence [34–36], or the heterogeneous bursty interaction dynamics [30,34,35,37] all have been identified to be important in influencing spreading processes on temporal networks.

However, these studies usually focus on either simple or complex contagion mechanisms to explain the actual spreading phenomena. Some aim to differentiate between these

*Contact author: karsaim@ceu.edu

mechanisms from a global view [38,39] or from local knowledge only [40] or by studying their coevolution [41]. In other works, contagion mechanisms vary across network layers or by communities [42,43], while some other models assign individual thresholds to nodes, specifying the number of exposures needed for adoption [31,44–47]. The infectiousness of the spreading process and the underlying network structure often determine which mechanism dominates the unfolding process [48]. In the case of mixed simple and complex contagion processes, the more easily contracted simple contagion may govern the spreading initially but in turn could trigger the complex contagion process, where the infection of an ego is conditional to a larger fraction of prior infected peers [47].

In some of these studies, even though both simple and complex contagions coexist in one spreading process, nodes are always assigned a predefined mechanism. In some cases, the contagion dynamics is determined by the community or network layer membership, while in others it depends on a predefined infectiousness threshold specific to each node. In contrast, in real-world scenarios, individuals are not limited to a single contagion mechanism: they might adopt through both simple and complex contagions depending on the social context. For example, adoption of a product might occur from a single intimate contact (simple contagion) or through repeated interactions with distant acquaintances (complex contagion). Therefore, the consideration of the interplay between these mechanisms is pivotal to understanding real social contagion phenomena better. Moreover, while the important effects of time-varying interactions on spreading processes have been well established, studies mixing simple and complex contagions on temporal networks are scarce, as early works have been limited to static networks.

In this paper, we address this knowledge gap by proposing an approach to model processes with multiple adoption mechanisms on temporal networks. In our model, a node is not endowed with a preassigned contagion mechanism but it could adopt via either a simple or a complex contagion. Our goal is to propose methods to identify whether simple, complex, or mixed contagion processes dominate the early and late dynamics of the modeled spreading process with mixed mechanisms. We classify processes into three categories, each corresponding to a distinct phase in the space of relevant parameters, and propose methods to identify the boundaries between these phases.

II. MODEL DEFINITION

We simulate the dynamics of time-varying interactions by building on the activity-driven network (ADN) model, that provides a flexible modeling framework of temporal networks [12,49,50]. We consider N initially disconnected nodes, each of them assigned with an activity $a_i \in [0, 1]$, extracted from an arbitrary distribution $F(a)$. The network evolves through asynchronous iterations of N microscopic time steps, during which each node is updated once on average. In a single microscopic time step, of duration $\Delta t = 1/N$, a node i is selected randomly and it becomes activated with probability a_i [51]. In the case of activation, the node connects to m randomly selected other nodes from the network, avoiding self-loops and multilinks. In the following iteration, we delete all links and start the process over again.

To model a binary-state contagion process [13] on the top of an ADN model, we assume that each node at any time step can be in one of two mutually exclusive states: susceptible (S), thus not yet reached by the contagion process, or infected (I) if it has been contaminated. We set all nodes initially as susceptible and start the spreading from a small set of randomly selected infected seed nodes. Once a susceptible node is contaminated during the spreading, it remains in this state; thus the system is evolving towards a fully infected absorbing state. Susceptible nodes can become infected in two ways: either get contaminated through the *simple contagion* mechanism, with an independent probability β for each contact with an infected peer, or through the *complex contagion* mechanism, if the fraction of infected neighbors exceeds a threshold $\phi \in [0, 1]$, preassigned to each node. The simple contagion is thus driven by a stochastic process, while the complex contagion is fully deterministic, ruled by the threshold and the proportion of infected neighbors of each node at each time step.

We initially infect a randomly selected 1% of seed nodes. Subsequently, at each time step, if an activated node is susceptible, it will follow the simple contagion mechanism with probability p, and thus it may get infected with probability β from any of its infected neighbors. Otherwise, with probability $1 - p$, the node will follow the complex contagion rule; thus it gets infected if the fraction of the infected neighbors exceeds the threshold ϕ [52]. In practical terms, if n_i is the number of infected nearest neighbors of the susceptible node i, complex contagion takes place if $n_i \geqslant z$, where $z = \lceil m\phi \rceil$. These steps are repeated until every node is in the infected state.

In the following, we denote by $I(t)$ the number of infected nodes at time t and by $\rho(t) = I(t)/N$ (ρ for brevity) the fraction of infected nodes (prevalence), while ρ_0 indicates this quantity at the start of the propagation. Likewise, ρ_s and ρ_c indicate the fractions of nodes infected by the simple or complex contagion, respectively. To simplify the mathematical description, we formulate some assumptions about the propagation process. We model a homogeneous network dynamics by assuming that all nodes have the same activity a, while we consider the heterogeneous case in Fig. 2. Further, we study the cases of $z = 2$ and $z = 3$; in other words, when susceptible nodes need two, or in another case three infected neighbors to adopt. The analytical treatment for more general cases with any value of z is outlined in the Appendix D.

III. ANALYTICAL STUDY

To shed analytical light on the model, we consider its description in terms of a mean-field rate equation, inspired by Ref. [49], for the fraction of infected nodes $\rho(t)$. In our description we take into account the effects of activity and the two alternative methods of infection, either simple or complex contagion; see Appendix A.

We first consider the case where only complex contagion is present, corresponding to $p = 0$. The exact rate equation cannot be easily solved analytically. Therefore, in order to get some insight into the dynamics, we focus on its early time evolution, when $\rho \ll 1$, corresponding to a leading order

expansion (see Appendix B). In this regime, the density of infected nodes follows the equation

$$\rho^{z-1}(t) = \frac{1}{\rho_0^{1-z} - (z-1)C\,t}, \tag{1}$$

where C is a constant depending on a, m, and $z = \lceil m\phi \rceil$, which we assume to be larger than 1. This function shows a linear decrease in time of the quantity $1/\rho^{z-1}$, and a divergence at time $t = \rho_0^{1-z}/[C(z-1)]$. This divergence is nonphysical since it appears as a lower-order approximation; adding other terms in the full equation curbs the divergence and leads to a prevalence $\rho(t) \leqslant 1$. However, we can interpret this apparent divergence in opposition to the behavior of pure simple contagion, in which prevalence grows exponentially in the linear approximation [16]. Complex contagion operates instead in cascades, in which a large fraction of nodes become infected in a very short period of time [19]. Thus, we can identify the divergence time as the onset of the cascading behavior of complex contagion.

When both simple and complex contagions are present ($0 < p < 1$), and focusing on the case $z = 2$, the evolution of the prevalence reads as

$$\frac{d\rho}{dt} = a\,p\,m\,\beta\,(\rho + B\,\rho^2), \tag{2}$$

up to order ρ^2, where we have defined the constant $B = \frac{(1-p)(m-1)}{2p\beta} - \frac{(m-1)\beta}{2} - 1$ (for further details see Appendix C). The solution of Eq. (2) in terms of the initial density of infected nodes is

$$\rho(t) = \frac{1}{A\,e^{-a\,p\,m\,\beta\,t} - B}, \tag{3}$$

where $A = B + \frac{1}{\rho_0}$. The sign of B determines the behavior of the prevalence: for $B < 0$, $\rho(t)$ has a monotonous behavior, while for $B > 0$, $\rho(t)$ shows again a divergence. Within the higher-order approximation, this can be understood at negative B, corresponding to simple contagion, and positive B to complex contagion. The transition between those two regimes arises when $B = 0$, yielding the critical value of p separating the regimes:

$$p_c(\beta) = \frac{m-1}{2\beta + (1+\beta^2)\,(m-1)}. \tag{4}$$

If B is positive, the prevalence diverges at

$$t_{\text{casc}} = \frac{1}{a\,p\,m\,\beta}\,\ln\left(\frac{A}{B}\right), \tag{5}$$

which serves as a proxy of the time of onset of the cascading behavior in complex contagion.

Finally, for $B > 0$, by analyzing the evolution of Eq. (2), we can calculate when the first term on the right-hand side (rhs), corresponding to pure simple contagion, is equal to the second term, with contributions of both the simple and complex contagions. These terms are equal at the prevalence

$$\rho_{\text{eq}} = 1/B, \tag{6}$$

which corresponds to the time

$$t_{\text{eq}} = \frac{1}{a\,p\,m\,\beta}\,\ln\left(\frac{A}{2B}\right). \tag{7}$$

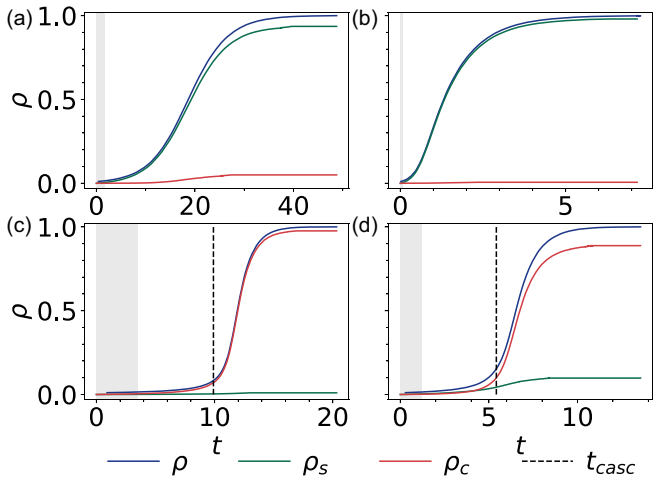

FIG. 1. Fraction of all infected nodes ρ (blue line) together with the fraction of nodes infected by simple ρ_s (green) and complex ρ_c (red) contagion as a function of time, for $z = 2$. Panels show different (β, p) parameters: (a) (0.05, 0.99), (b) (0.99, 0.99), (c) (0.05, 0.05), and (d) (0.99, 0.05). The simple (complex) contagion dominates the propagation when p is high (low), with a minor influence from β, which can be observed in Fig. 5. The gray area indicates the early period of the contagion up to t_{init}, when $\rho = 0.02$. Dashed vertical lines show t_{casc}, corresponding to the expected outbreak time if B is positive [see Eq. (5)], in panels (c), (d).

At this time, complex contagion takes over the initial simple contagion dynamics, in the complex dominated regime $p < p_c(\beta)$, a phenomenon, which has already been identified previously [47].

IV. NUMERICAL SIMULATIONS

We compare our analytical results with numerical simulations, using parameters $N = 1000$, $a = 1$, $m = 5$, and $\phi = 0.25$ for $z = 2$, and $\phi = 0.5$ for $z = 3$. We follow a Monte Carlo approach, averaging simulations over 100 independent runs. Specifically, we compute the average time required to reach each value of the number of infected nodes, that we normalize with N to obtain the average fraction of infection as a function of time. We fix $z = 2$ (if not noted otherwise) while varying β and p.

Figure. 1 shows the contagion curves for different β and p; for the full parameter space see Appendix E. When p is large, the dynamics is determined by simple contagion, as we can see by the rapid growth of the prevalence, which is faster for larger values of β [see Figs. 1(a) and 1(b)]. When p is small, on the other hand, the complex contagion prevails [see Figs. 1(c) and 1(d)]. In this regime, the prevalence grows initially slowly, followed by a sudden increase indicative of a cascade. Interestingly, as shown in Fig. 1(d), the ρ_c cascade emerges earlier when rare ($p = 0.05$) but likely transmitting ($\beta = 0.99$) simple contagion events are present. Since the initial seeds may not be eligible to induce a complex contagion outbreak, simple contagion cases build up the necessary initial conditions to trigger a complex contagion cascade.

Figure 1, and Fig. 5 in Appendix E, show that the analytically determined divergence time t_{casc} generally predicts quite

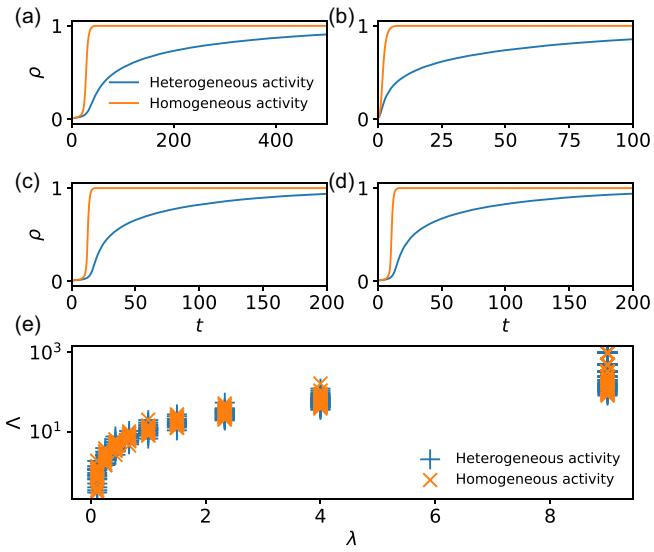

FIG. 2. Comparison of contagion curves panels (a)–(d) and the initial ratio λ vs the final infected ratio Λ (e) when all nodes have the same activity (homogeneous activity—blue curves and markers) and when the activities are sampled from a power-law distribution (heterogeneous activity—orange curve and markers). The simulations on panels (a)–(d) are parametrized with (β, p): (a) $(0.05, 0.99)$, (b) $(0.99, 0.99)$, (c) $(0.05, 0.05)$, and (d) $(0.99, 0.05)$. The propagation is considerably slower when the nodes have heterogeneous activities. At the same time, the observed Λ and λ values are very similar for the two activity distributions.

closely the time when the infection curve $\rho(t)$ starts taking off, signaling the onset of the cascades. Nevertheless, t_{casc} slightly underestimates the real outbreak time if both β and p have high values, while t_{casc} is somewhat late if β is low and p is high.

Further, we note that a nonconstant activity distribution can affect the propagation speed. We consider in Fig. 2 the case of heterogeneous activities by comparing the results of two activity distributions: a Dirac distribution $\delta(a)$ (every node has the same activity) and a power-law distribution $P(a) \sim a^{-\gamma}$. Both distributions have the same average of $\langle a \rangle = 0.1$; thus the exponent of the power law is $\gamma = 1.14$. Figures 2(a)–2(d) show that when activities are drawn from a power-law distribution, the epidemic takes longer to reach every node, as compared to the case when all nodes have the same activity.

Following this qualitative analysis, we now focus on disentangling the effective mechanisms that rule the evolution of the spreading process. As we have mentioned above, the dominant mechanism can change during the process in the mixed simple and complex scenario. We thus consider the early and late stages of the propagation separately. The early stage is defined for times smaller than t_{init}, at which the prevalence ρ fulfills the condition $\rho(t_{\text{init}}) = 0.02$, while the late stage starts at t_{init} and runs to the time when all nodes are infected, t_{end}. The results presented in the following are robust over a range of values t_{init}, as discussed in Appendix F. To identify the early and late contagion mechanisms we consider the ratios $\lambda = \rho_c(t_{\text{init}})/\rho_s(t_{\text{init}})$ and $\Lambda = \rho_c(t_{\text{end}})/\rho_s(t_{\text{end}})$. If the simple (resp. complex) contagion dominates the entire process, both quantities remain below (resp. above) 1. If the simple contagion dominates the early stage but the complex one takes over in the late stage, then we expect $\Lambda > 1$ and $\lambda < 1$, respectively.

Since the case $\Lambda < 1$ and $\lambda > 1$ cannot be observed (once the complex contagion is triggered, it propagates much faster than the simple one), we classify the spreading dynamics into three categories: pure simple contagion ($\Lambda < 1$ and $\lambda < 1$), pure complex contagion ($\Lambda > 1$ and $\lambda > 1$), and mixed contagion ($\Lambda > 1$ and $\lambda < 1$). We thus expect two transitions in the parameter space (β, p). The first, from pure simple to mixed contagion, and the second from mixed to pure complex. The first transition takes place at a threshold $p_c(\beta)$, given by Eq. (4) for $z = 2$, separating the phase in which simple contagion is dominating asymptotically from the phase in which complex contagion dominates at large times. In the mixed phase, while complex contagion is dominant at late times, at the early phase simple contagion is prevalent. The second transition separates this mixed phase from the pure complex contagion phase, in which even at early times complex contagion is predominant. Changing homogeneous activity to heterogeneous does not significantly affect the outcome of the propagation dynamics: the initial and final ratios of nodes infected by the simple and the complex contagions are very similar [see Fig. 2(e)].

In the following, we propose two different methods to identify the transition point from mixed to pure complex phases:

Method 1. In the complex contagion dominated phase, we measure the time t_{eq} and prevalence $\rho_{\text{eq}} = \rho(t_{\text{eq}})$ when the two terms in the rhs of Eq. (2) become equal, indicating when the simple contagion term takes over the complex contagion one. These quantities can be computed analytically from Eqs. (6) and (7), and numerically by evaluating in simulations when the first and second terms in the rhs of Eq. (2) become equal. The time t_{eq} signals the transition between a dynamics initially dominated by simple contagion and the dynamics asymptotically dominated by complex contagion. In the parameter space (β, p), the transition from the mixed phase to the pure complex contagion phase should thus correspond to $t_{\text{eq}}(\beta, p) = 0$ (noted t_{eq} *null* in the following figures), that is, when right at the initial time step the contagion is dominated by the complex mechanism.

Method 2. The second approach relies on the results in Eq. (1), suggesting that the function $1/\rho^{z-1}$ should decrease linearly with time t, if the spreading is governed by pure complex contagion. We demonstrate this behavior in Figs. 3(b) and 3(c) by showing the curve $1/\rho^{z-1}$ for simulations (dark blue line) with parameters $(p, \beta) = (0.07, 0.07)$ and $(p, \beta) = (0.4, 0.4)$, corresponding to the (β, p) pairs indicated by the black points in Fig. 3(a). In the case where both simple and complex contagions are present, the early time behavior of $1/\rho^{z-1}$ scales also linearly with t. This is evident from Eq. (3), as it can be seen expanding the exponential in the denominator using its Taylor series regardless of the sign of B. However, this linear trend breaks down earlier, since the expansion of the exponential fails sooner. As a result, the complex contagion dominates longer, as marked by a longer linear decrease. To quantify this effect, we first consider an initial regime up to small initial time t_{init}, in which we assume a linear behavior for $1/\rho^{z-1}$ [Figs. 3(b) and 3(c), gray area]. To take equally different values of z, we define t_{init} as the time when ρ

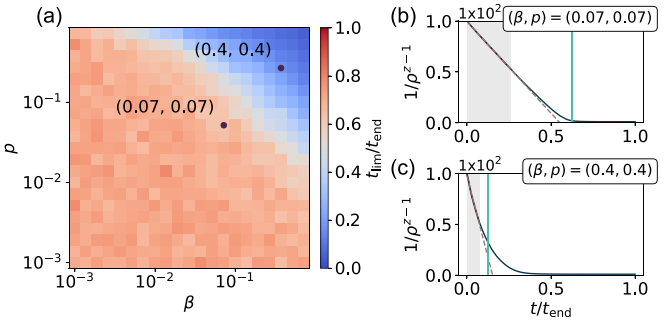

FIG. 3. The ratios $t_{\text{lim}}/t_{\text{end}}$ obtained across the whole parameter space (β, p) for $z = 2$ (a) and the $1/\rho^{z-1}$ curves (dark blue line) obtained from simulation averages with $(\beta, p) = (0.07, 0.07)$ (b) and $(\beta, p) = (0.4, 0.4)$ (c). These curves are fitted by a linear function (black dotted line) on the period before t_{init} (gray area). The t_{lim} time point corresponds to an $\epsilon > 0.15/\rho_0^{z-1}$ difference when the two curves diverge, as indicated by a vertical light blue line. $1/\rho^{z-1}$ stops being linear at early times when the propagation is fast, i.e., when both β and p are high, while this linearity persists longer when the contagion process is slow (low β and p). Simulations results were calculated as averages over 100 realizations.

satisfies the condition $\frac{1}{\rho^{z-1}(t_{\text{init}})}/\frac{1}{\rho_0^{z-1}} = 0.5$, which corresponds to $\rho(t_{\text{init}}) = 0.02$ if $z = 2$ and $\rho_0 = 0.01$. We then fit a linear function to $1/\rho(t)^{z-1}$ in the interval $[0, t_{\text{init}}]$ [Figs. 3(b) and 3(c), black dotted line]. Finally, we identify the value t_{lim} at which the linear behavior breaks down, indicated by a vertical light blue line. This is defined by the time at which the function $1/\rho(t)^{z-1}$ differs from the initial linear fit by a value larger than or equal to $\epsilon = \alpha/\rho_0^{z-1}$, $\alpha = 0.15$. The parameter α can be chosen in a broad range $[0.1, 0.5]$ leading to similar results; see Appendix F. The prevalence at this time is denoted as $\rho_{\text{lim}} = \rho(t_{\text{lim}})$.

We display the rescaled time $t_{\text{lim}}/t_{\text{end}}$ for an extended parameter space in Fig. 3(a). According to these results our method can well separate the regime where the complex contagion dominates (characterized by large $t_{\text{lim}}/t_{\text{end}}$ values and corresponding to lower values of β and p), from the simple contagion dominated regime (with small values of $t_{\text{lim}}/t_{\text{end}}$ and for higher values of β and p).

In Fig. 4, in the (β, p) parameter space, we show how the proposed analytical and numerical methods capture the transitions from pure simple contagion to mixed, and from mixed to pure complex contagion. In Figs. 4(a) and 4(b) [resp. 4(c) and 4(d)] we show results for the $z = 2$ (resp. $z = 3$) case. The regions are determined by comparison of the values λ and Λ defined above: pure simple contagion for $\Lambda, \lambda < 1$; pure complex contagion for $\Lambda, \lambda > 1$; and mixed contagion for $\Lambda > 1$, $\lambda < 1$. For $z = 2$ [see Fig. 4(a)], the phase boundary between pure complex (brown area) and mixed (pink area) is well captured by method 1, corresponding to a null t_{eq} line in red. The boundary between mixed and pure simple (green area) is slightly shifted from the prediction $p_c(\beta)$ (green line). In the case of $z = 3$ [see Fig. 4(c)], again method 1 provides an excellent approximation for the boundary between pure complex and mixed phases, which seems to take place at smaller values of (β, p) than for $z = 2$. In this case, we do not have an analytical prediction for the boundary of mixed and pure

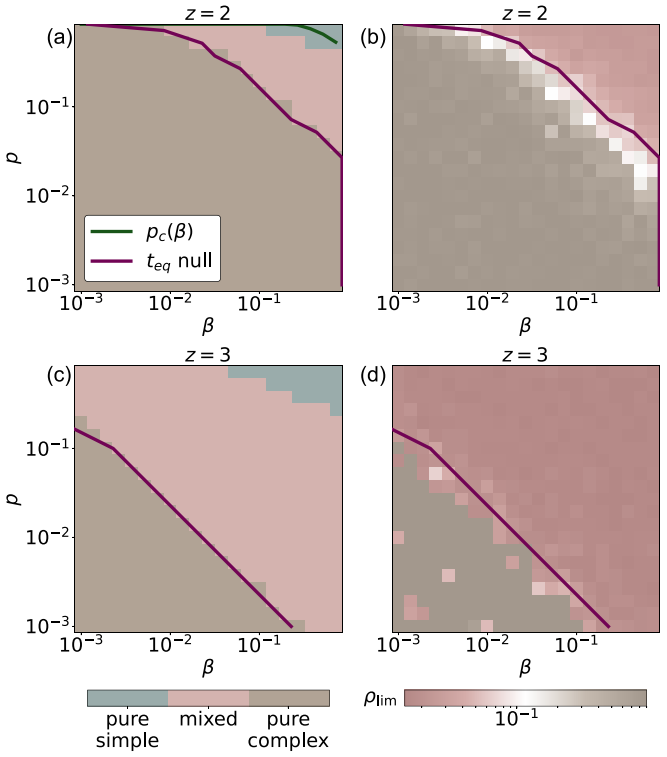

FIG. 4. Areas corresponding to the three categories in the parameter space (β, p) in (a) for $z = 2$ and in (c) for $z = 3$. The $p_c(\beta)$ curve (dark green) and the limiting curve of t_{eq} null (dark red) match well the transitions between the different phases. The values of ρ_{lim}, displayed in (b) for $z = 2$ and (d) for $z = 3$. They reflect well the transition between the pure complex and mixed phases that collapse on the corresponding t_{eq} null (dark red) curve. Simulations were performed using parameters $N = 1000$, $\rho_0 = 10$, with results averaged over 100 independent realizations.

simple phases, leaving us alone with the results of numerical simulations. However, it seems to appear for smaller (β, p) values as compared to the corresponding $z = 2$ case.

In Figs. 4(b) and 4(d), we present the predictions of method 2 for the location of the boundaries between pure complex and mixed phases for the cases of $z = 2$ [Fig. 4(b)] and $z = 3$ [Fig. 4(d)], respectively. In these plots we show the density ρ_{lim} for the whole range of the (β, p) parameter space, as color maps. We found an excellent match of the phase boundary extracted from method 2 and the classification made in terms of Λ and λ ratios displayed as a color map for $z = 2$ [Fig. 4(a)] and $z = 3$ [Fig. 4(c)]. Further, these boundaries closely recover the prediction of method 1 represented by the t_{eq} null curve (dark red line) on each figure.

V. CONCLUSION

Social contagion processes are mediated by temporal interactions of individuals who may follow simple or complex contagion mechanisms to adopt. Meanwhile, the actual mechanisms may vary between people and from one adoption case to another, depending on the spreading item and the social context. These aspects were overlooked by earlier studies, which to model mixed spreading processes, usually predefined

contagion mechanisms for each individual and focused on their spreading only on static networks. This work closes this existing gap by introducing a mixed model of social contagion on temporal networks, in which nodes can be infected by either simple or complex contagion dynamics simultaneously. We focused on the simplest modeling scenario of a homogeneous activity-driven network with all nodes having the same activity. We tackled the solution of the model analytically using mean-field rate equations for the total density of infected nodes as a function of time, and numerically through extensive simulations. We also explored numerically heterogeneous activity systems. This way we proposed two ways to differentiate between processes of different dominant contagion processes at the early and late stages of the spreading dynamics.

We identified three phases of contagion according to the two main parameters of the model, the probability p of adopting by simple contagion, and the infection probability β of simple contagion. We found that for small values of (β, p), the dynamics is ruled purely by complex contagion. For intermediate values instead, the dynamics is mixed: initially dominated by simple contagion but following complex contagion at later times. Finally, for large (β, p) parameter values the spreading is dominated by the simple contagion mechanism. We proposed a criterion to determine these phases, that we confirmed by analytical expressions determining one of the phase boundaries, and by numerical methods for all of them.

The methodology presented here certainly has some limitations. While we found these results robust and very similar to adoption dynamics on networks with heterogeneous activities, the analytical approach is only valid when all the nodes have the same activity. Also, the chosen binary-state model is simplistic and could be further extended using more realistic contagion models such as multistate spreading models [53]. Finally, as our work is exploratory, it may not be readily applicable for real systems, where neglected dynamical characters like burstiness or causal event correlations [37] play roles and complicate the observations of the adoption mechanisms.

Future work should be dedicated to extending the analytical study to larger z values, and to find a critical adoption probability p_c separating simple and mixed contagion in these cases. Furthermore, we explored the effect of heterogeneity of nodes—with respect to their activity rate—only qualitatively, by comparing contagion curve profiles between constant and power-law activity distributions. Extending the analytical and numerical frameworks presented here to temporal networks with heterogeneous activities, as well as exploring the effect of bursty interaction patterns [54] on the mixed contagion dynamics represent significant venues for future research.

ACKNOWLEDGMENTS

M.S. acknowledges support from Grants No. RYC2022-037932-I and No. CNS2023-144156 funded by MCIN/AEI/10.13039/501100011033. R.P.-S. Acknowledges financial support from Project No. PID2022-137505NB-C21/AEI/10.13039/501100011033/FEDER UE. M.K. acknowledges funding from the National Laboratory for Health Security (Grant No. RRF-2.3.1-21-2022-00006); the DATAREDUX (Grant No. ANR-19-CE46-0008); the SoBigData++ H2020-871042; the SoBigData PPP: HORIZON-INFRA-2021-DEV-02 project (Grant No. 101079043); the COLINE FFG-DTU; and the MOMA WWTF projects.

APPENDIX A: MEAN-FIELD RATE EQUATION

We consider the time evolution of the number of infected individuals $I(t)$. In a microscopic time step Δt, we choose a node at random (the ego node), which is susceptible with probability $(N - I)/N$. The ego node becomes active with probability a, in which case with probability p it follows a simple contagion, and with probability $1 - p$ it follows a complex contagion to potentially become infected. Therefore, within a mean-field approximation [49], the number of infected nodes at time $t + \Delta t$ can be written as

$$I(t + \Delta t) = I(t) + \frac{N - I(t)}{N} a\,[p\,\Delta_{m,\beta}(\rho) + (1 - p)\,P_z(\rho)], \tag{A1}$$

where $\Delta_{m,\beta}(\rho)$ and $P_z(\rho)$ are the probabilities that the focal node becomes infected by the simple and complex processes, respectively. For the simple contagion process, the ego node is connected to m other nodes, each one infected with probability ρ. Each infected neighbor transmits the infection to the ego node with probability β. Thus, the probability that any one of the infected neighbors infects the ego is

$$\Delta_{m,\beta}(\rho) = 1 - (1 - \rho\,\beta)^m. \tag{A2}$$

On the other hand, for complex contagion to take place, we need the ego to be the neighbor of at least z infected nodes, an event that happens with probability

$$P_z(\rho) = \sum_{n=z}^{m} \binom{m}{n} \rho^n (1 - \rho)^{m-n} \equiv \mathrm{I}_\rho(z, m + 1 - z), \tag{A3}$$

where $\mathrm{I}_x(a, b)$ is the regularized incomplete beta function [55].

Assuming that the time interval $\Delta t = 1/N$, in such a way that a whole update of the network corresponds to one Monte Carlo time step, we can take the thermodynamic limit $N \to \infty$ in Eq. (A1) to write the differential rate equation

$$\frac{d\rho}{dt} = a\,(1 - \rho)\,[p\,\Delta_{m,\beta}(\rho) + (1 - p)\,P_z(\rho)]. \tag{A4}$$

In the following, we analyze the beginning of the propagation process, in the limit $t \to 0$, $\rho \ll 1$, considering different cases.

APPENDIX B: PURE COMPLEX CONTAGION

The case when all nodes follow the complex contagion mechanism corresponds to $p = 0$. In this scenario, using Eqs. (A4) and (A3), we obtain

$$\frac{d\rho}{dt} = a\,(1 - \rho)\,I_\rho(z, m + 1 - z). \tag{B1}$$

Since we are interested in the behavior for small t and ρ, we can use the power expansion of the regularized incomplete

beta function for integer z [55]:

$$I_\rho(z, m+1-z) \sim \rho^z \binom{m}{z}, \quad \rho \to 0. \tag{B2}$$

Thus, keeping only the leading terms, Eq. (B1) can be written as

$$\frac{d\rho}{dt} = C\rho^z, \tag{B3}$$

where the constant C is equal to

$$C = a\binom{m}{z}. \tag{B4}$$

The solution of this equation, in terms of the initial density of infected seeds ρ_0, is

$$\rho^{z-1}(t) = \frac{1}{\rho_0^{1-z} - (z-1)\,C\,t}. \tag{B5}$$

This solution shows a linear decreasing behavior in time of the function $1/\rho^{z-1}$, with a divergence at a time $t = \rho_0^{1-z}/[C(z-1)]$. The time of the divergence is smaller when ρ_0 is higher, as initially there are more infected nodes, and when z is smaller, as the condition to be infected is easily reached.

The fact that the density of infected nodes exhibits a singularity at the small time description can be interpreted as a signature of the complex contagion mechanism, which usually proceeds in cascades in which a large fraction of nodes become infected in a very short period of time [19]. This behavior is in contrast with simple contagion, which at short times is defined by a monotonous exponential increase.

APPENDIX C: MIXED SIMPLE AND COMPLEX CONTAGION

We consider now the case of mixed simple and complex contagions. To simplify our calculations, we focus here on the case of $z = 2$. We thus have, for the simple contagion infection probability,

$$\Delta_{m,\beta}(\rho) = 1 - (1-\rho\,\beta)^m \simeq m\,\beta\,\rho - \rho^2\,m\,(m-1)\frac{\beta^2}{2}, \tag{C1}$$

where we have kept only the lower-order terms in ρ. For the complex contagion probability, from Eq. (B2),

$$P_2(\rho) \simeq \rho^2 \binom{m}{2} = \rho^2\,\frac{m\,(m-1)}{2}, \tag{C2}$$

where again we have kept only the leading terms in ρ. Inserting Eqs. (C1) and (C2) in Eq. (A4), we obtain

$$\frac{d\rho}{dt} = a\,p\,m\,\beta\,(\rho + B\,\rho^2) \tag{C3}$$

up to order ρ^2, and where we have defined the constant

$$B = \frac{(1-p)\,(m-1)}{2\,p\,\beta} - \frac{(m-1)\,\beta}{2} - 1. \tag{C4}$$

The solution of Eq. (C3) in terms of the initial density of infected nodes is

$$\rho(t) = \frac{1}{Ae^{-t\,a\,p\,m\,\beta} - B}, \tag{C5}$$

where we have defined the constant:

$$A = B + \frac{1}{\rho_0}. \tag{C6}$$

If B is negative (and ρ_0 sufficiently small in such a way that $A > 0$), then $\rho(t)$ grows at short times, until it saturates to the value $1/|B|$. If B is positive, on the other hand, $\rho(t)$ diverges at the time

$$t_{\text{casc}} = \frac{1}{a\,p\,m\,\beta}\,\ln\left(\frac{A}{B}\right), \tag{C7}$$

which serves as a proxy to indicate the time of the cascade, namely, the time of a sudden increase of the density of infected nodes.

These different behaviors, depending on the sign of B can be understood as follows. For $B < 0$, the second term on the rhs of Eq. (C3) is negative, in agreement with the second-order expansion of the rate equation for pure simple contagion [see Eq. (C1)]. Otherwise, if $B > 0$, the second term on the rhs of Eq. (C3) is positive, as it corresponds to the pure complex contagion rule [see Eq. (C2)]. We can interpret the value $B = 0$, corresponding to the probability

$$p_c(\beta) = \frac{m-1}{2\,\beta + (1+\beta^2)\,(m-1)}, \tag{C8}$$

as the boundary separating a dominating simple contagion (for $p > p_c$) from a dominating complex contagion (for $p < p_c$). Within the complex contagion dominated phase, the divergence time t_{casc} is a proxy of the time at which complex contagion takes over from the simple contagion prevalent at very short times.

The divergence time t_{casc} diminishes as ρ_0 increases, since the increase of the proportion of infected nodes occurs earlier when there are initially more infected nodes. The parameter β also makes the critical time decreasing when it is increasing: as there is a higher probability to be infected for the simple contagion, the number of infected nodes is greater; thus the increase of ρ is earlier.

In the complex contagion dominated region with $B > 0$, another way to estimate when this dynamics takes over simple contagion emerges from the analysis of Eq. (2). In this equation, we have a linear term, arising from simple contagion, and a quadratic term, with components from the complex and simple contagions. Assuming that complex contagion dominates over simple contagion when the second-order term becomes larger than the linear one, we can define the threshold density of infected nodes,

$$\rho_{\text{eq}} = \frac{1}{B}, \tag{C9}$$

such that at the time t_{eq}, corresponding to $\rho(t_{\text{eq}}) = \rho_{\text{eq}}$, the second-order term overcomes the first-order one, and we expect complex contagion to prevail. From the solution Eq. (C5), we can estimate, within the small time approximation, and assuming ρ_0 is small enough such that $\rho_0 B < 1$,

$$t_{\text{eq}} = \frac{1}{a\,p\,m\,\beta}\,\ln\left(\frac{A}{2\,B}\right), \tag{C10}$$

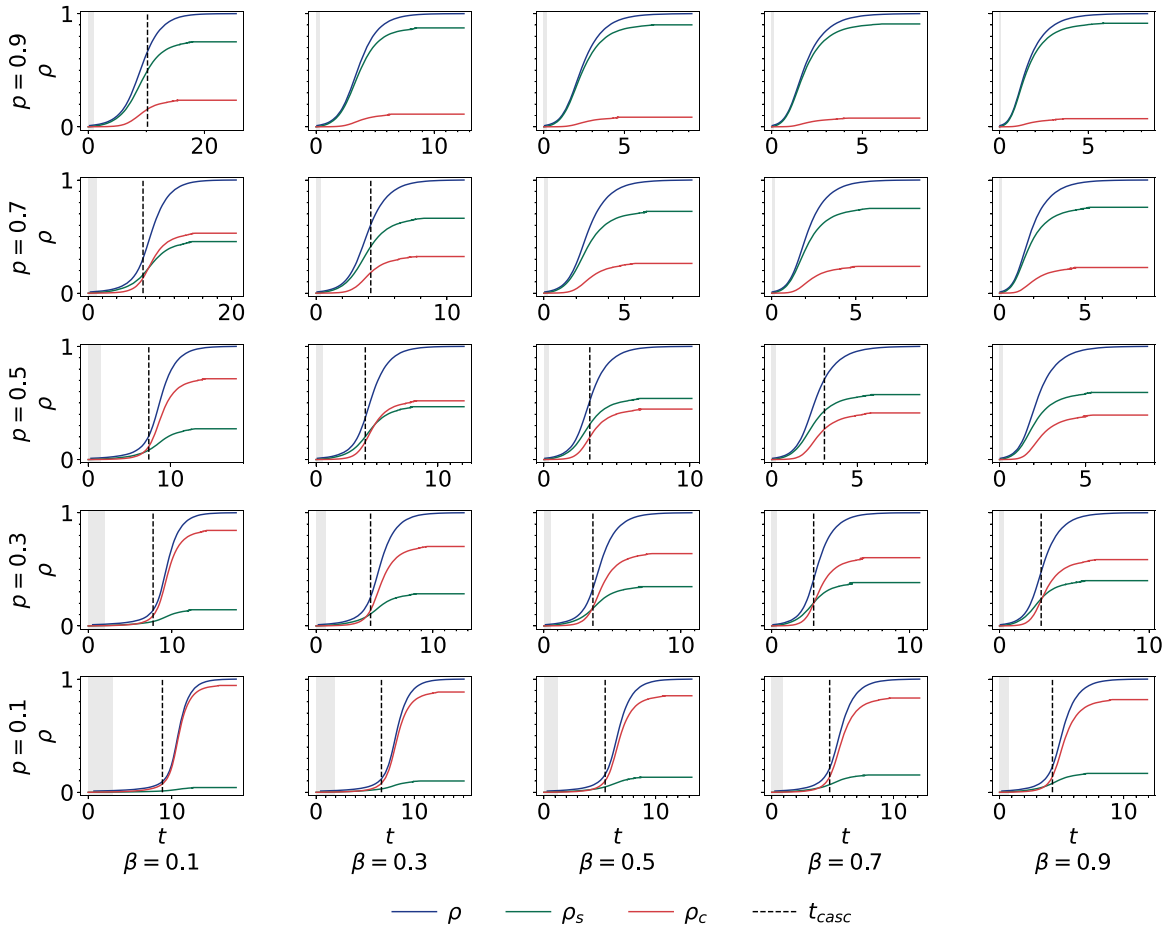

FIG. 5. Fraction of infected nodes, $\rho(t)$, as the function of time for simulated spreading scenarios (blue line), together with the proportion of nodes infected by the simple, ρ_s (green curve), and the complex, ρ_c (red curve), contagions for $z = 2$. Panels show simulation results averaged over 100 realizations, for different values of β (x axis) and p (y axis).

such that $t_{\text{eq}} < t_{\text{casc}}$. In the case that $\rho_0 > \rho_{\text{eq}}$, the quadratic term containing elements from the complex and simple contagions dominates from the initial instant of the dynamics. This scenario corresponds to $t_{\text{eq}} = 0$ and marks the region below which the complex contagion is fully predominant from the early stage of the dynamics.

To sum up the behavior of $z = 2$, for $p > p_c(\beta)$, contagion is dominated by the simple mechanism. For $p < p_c(\beta)$, contagion is dominated, at large times by the complex mechanism. At short times, however, simple contagion is prevalent, since it has a larger average transmission. At the time t_{eq}, complex contagion takes over from the initially predominant simple mechanism.

APPENDIX D: GENERAL CASE $z > 2$

We can also calculate ρ_{eq} when $z > 2$. To do so, we first aim to calculate the expression of $P(n \geqslant z)$ and $\Delta_{m,\beta}(\rho)$ in the general case in which z can take any value. We first prove that $P(n \geqslant z)$ is a polynomial for which the zth-order Taylor expansion has a lower degree of z, meaning that $P(n \geqslant z)$ is governed by the term ρ^z. Indeed, the Taylor expansion of the term $(1-\rho)^{m-n}$ in Eq. (A3) gives the following:

$$P(n \geqslant z)(\rho) = \sum_{n=z}^{m} \binom{m}{n} \rho^n \left[1 + \sum_{i=1}^{z} \frac{(-1)^i \rho^i}{i!} \times (m-n)\dots(m-n-i+1) \right]. \tag{D1}$$

In order to prove that the lowest degree of $P(n \geqslant z)$ is z, we consider the term ρ^α, with $\alpha < z$, and demonstrate that its coefficient C_α is null. From Eq. (D1), if α is equal to 0, the coefficient is $1 - \binom{m}{0}\rho^0$, which is null; otherwise the coefficient C_α is the following:

$$C_\alpha = -\binom{m}{\alpha} - \sum_{n=0}^{\alpha-1} \binom{m}{n} \frac{(-1)^{\alpha-n}}{(\alpha-n)!} (m-n)\dots(m-\alpha+1). \tag{D2}$$

By reorganizing the terms, Eq. (D5) is then equal to

$$C_\alpha = -\binom{m}{\alpha} \left[-1 - \sum_{n=0}^{\alpha-1} \binom{\alpha}{n} (-1)^{\alpha-n} \right]. \tag{D3}$$

The right term of Eq. (D3) can be expressed as $-1 - [\sum_{n=0}^{\alpha} \binom{\alpha}{n}(-1)^{\alpha-n} 1^n - 1]$. Using the Newton's binomial, we

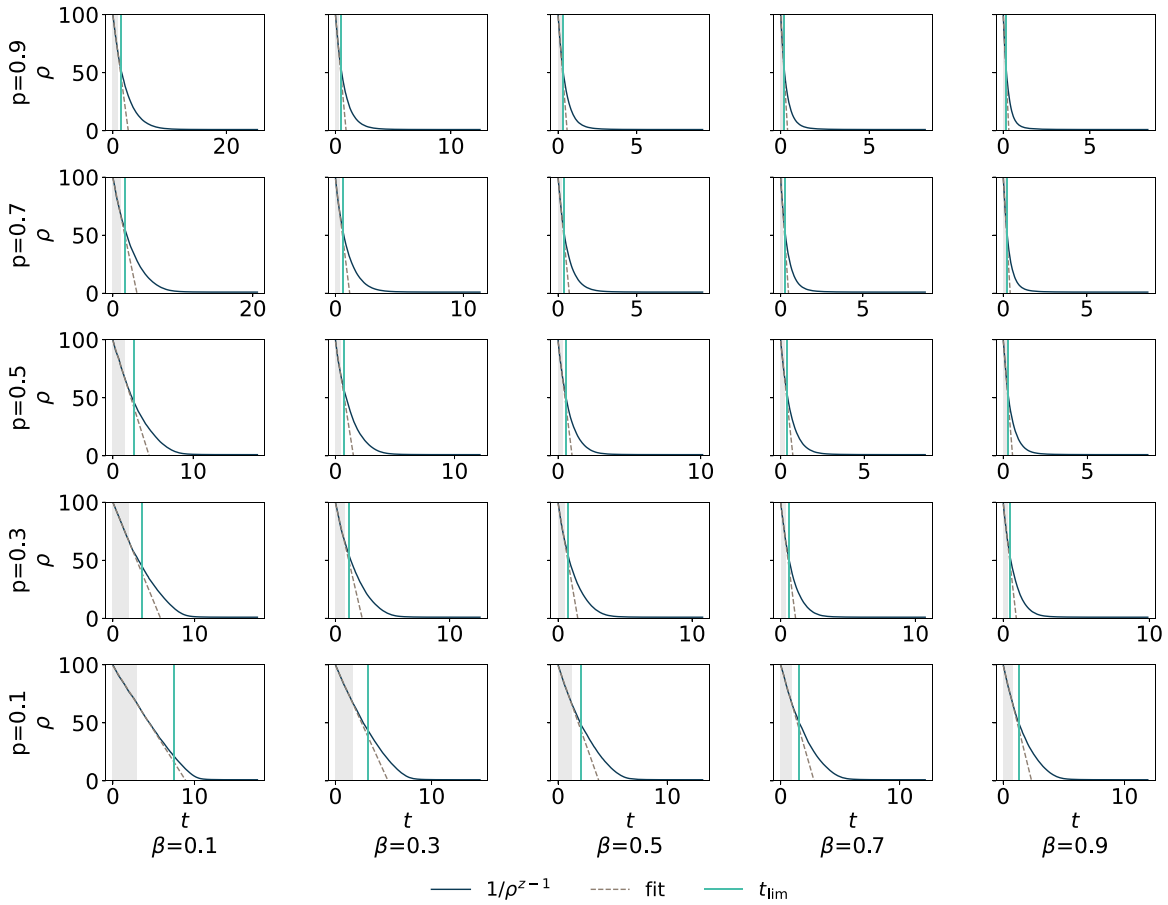

FIG. 6. Inverse of the proportion of infected neighbors to the power $z-1$ (dark blue line), fitted with a linear function on the first part of the propagation (black dotted line). The x axis stands for different values of β, while the y axis represents the values of p. The time t_{lim} when the difference between $1/\rho^z$ and its fit is higher than $\epsilon > 5$ is indicated with a light blue line.

show that that term is null, thus C^α is also null, which demonstrates that the zth-order Taylor expansion of the polynomial $P(n \geqslant z)$ has a lower degree of z. The coefficient of the term in z is then equal to

$$C_z = -\sum_{n=0}^{z-1} \binom{m}{n} \frac{(-1)^{z-n}}{(z-n)!} (m-n)\dots(m-z+1). \quad \text{(D4)}$$

By reorganizing the term, we prove that $C_z = \binom{m}{z}$, and then $P(n \geqslant z) = \binom{m}{z}\rho^z$.

The general term of $\Delta_{m,\beta}(\rho)$ is given by its Taylor expansion,

$$\Delta_{m,\beta}(\rho) = -\sum_{i=1}^{z} \binom{m}{i} (-1)^i \beta^i \rho^i. \quad \text{(D5)}$$

We then use those expressions in Eq. (A4). In the right part of the equation, the term in ρ^z is $a\binom{m}{z}[p(-\beta)^{z-1}[\beta + \frac{z}{m-z+1}] + 1 - p]\rho^z$ and the term in ρ is $-apm\beta\rho$. Those two terms are equivalent when

$$\rho_{\text{eq}} \approx \sqrt[z-1]{\frac{m\,p\,\beta}{\binom{m}{z}\left[p\,(-\beta)^{z-1}\left(\beta + \frac{z}{m-z+1}\right) + 1 - p\right]}}. \quad \text{(D6)}$$

APPENDIX E: SIMULATIONS ON THE EXTENDED PARAMETER SPACE (β, p)

The contagion curves and the expected times of increase t_{casc}, displayed in Fig. 2 in the main text for four different parametrizations (β, p), are shown for a larger range of values in Fig. 5. We can observe that large values of p and small values of β lead to a slow dynamics, as the model attempts but fails to infect nodes through the simple contagion. In contrast, the fastest contagion processes are for high values of both p and β as the nodes in this setting are mainly infected successfully by the simple contagion.

In the same figures, we also explore the proportion of nodes infected by each process through time, namely, ρ_s and ρ_c. Complex contagion dominates the propagation for small values of p, as nodes are more likely infected by the complex contagion in this setting. Also, in line with previous results, the simple contagion governs the spreading when p is high. The influence of β is minor but observable, leading to higher ρ_s when β increases. In particular, in the simulations for $p = 0.5$, $p = 0.6$, and $p = 0.7$, raising β changes the contagion process dominating the simulation, from the complex to the simple contagion.

Figure 6 exemplifies the second method to evaluate the dominance of the simple or complex contagion at the beginning of the process with an extended parameter space

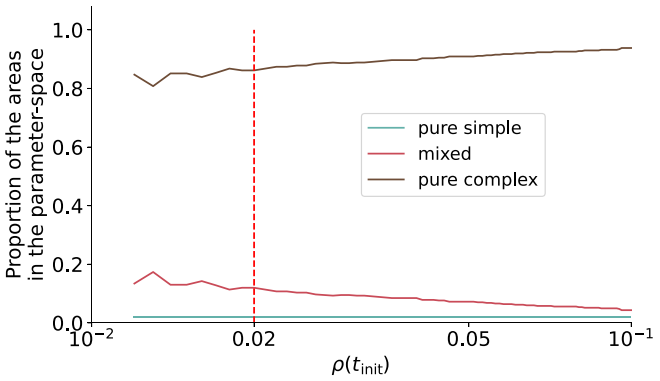

FIG. 7. Proportion of the areas of the three categories: pure simple (blue curve), mixed (pink curve) and pure complex (gray curve) over the whole parameter space (y axis) as a function of $\rho(t_{\text{init}})$. If $\rho(t_{\text{init}})$ is small, the areas of the three categories are very similar.

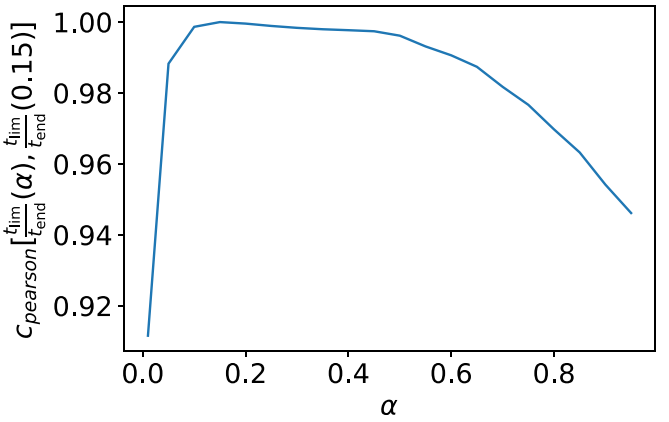

FIG. 8. Pearson coefficient (y axis) comparing the value of $t_{\text{lim}}/t_{\text{end}}$ over the entire phase space between the case $\alpha = 0.15$ and another value of α (x axis).

compared to Fig. 3 in the main text. The curve ρ^{z-1} is linear decreasing if the complex contagion dominates, which is the case for low values of β and p. We measure the linearity of the early times of the curves by fitting the curves with a line and showing the time when the simulations and the fits have a difference higher than ϵ. As expected, the linear trend is not present for high values of β and p, for which the simple contagion governs.

APPENDIX F: ROBUSTNESS WITH RESPECT TO t_{init} AND ϵ

We define the initial stage of the contagion process as the period up to the time t_{init}. The choice of t_{init} has a direct influence on the parameter λ, which determines the classification of the contagion dynamics into the three categories: pure simple, mixed, and pure complex. In the paper, we choose t_{init} such that $\rho(t_{\text{init}}) = 0.02$.

In Fig. 7, we assess the impact of the threshold $\rho(t_{\text{init}})$ on the results, by looking at the fraction of the three categories (pure simple, mixed, and pure complex) in the parameter space (β, p) (see Fig. 4), as a function of $\rho(t_{\text{init}})$. One can see that the fraction of the pure simple category remains low and constant regardless of the value of $\rho(t_{\text{init}})$, while the mixed category slightly declines and the pure complex category slightly increases as $\rho(t_{\text{init}})$ increases. Therefore, for small values of $\rho(t_{\text{init}})$ (e.g., $\rho(t_{\text{init}}) < 0.04$) results are very similar, indicating that the choice of $\rho(t_{\text{init}})$ does not affect the model's outcome in this range.

Similarly, we evaluate the impact of the parameter α on the threshold $\epsilon = \alpha/\rho_0^{z-1}$ ϵ for method 2, used to determined the end of the linear regime. In Fig. 8, we assess the impact of α, by comparing the ratio $t_{\text{lim}}/t_{\text{end}}$ across the whole parameter space between the case $\alpha = 0.15$ (used in the main paper) and alternative value of α using the Pearson correlation coefficient. The results indicate that for α values in the range [0.1, 0.5], the method yields very similar outcomes.

[1] N. A. Christakis and J. H. Fowler, Social contagion theory: examining dynamic social networks and human behavior, Stat. Med. **32**, 556 (2013).

[2] C. Castellano, S. Fortunato, and V. Loreto, Statistical physics of social dynamics, Rev. Mod. Phys. **81**, 591 (2009).

[3] S. Jose, Covid vaccine and generation z—a study of factors influencing adoption, Young Consumers **23**, 16 (2022).

[4] N. A. Christakis and J. H. Fowler, The collective dynamics of smoking in a large social network, N. Engl. J. Med. **358**, 2249 (2008).

[5] N. O. Hodas and K. Lerman, The simple rules of social contagion, Sci. Rep. **4**, 4343 (2014).

[6] F. M. Bass, A new product growth for model consumer durables, Manag. Sci. **15**, 215 (1969).

[7] E. M. Rogers, A. Singhal, and M. M. Quinlan, Diffusion of innovations, in *An Integrated Approach to Communication Theory and Research* (Routledge, Milton Park, UK, 2014), pp. 432–448.

[8] R. I. Dunbar, The social brain hypothesis, Evol. Anthropol.: News Issues Rev. **6**, 178 (1998).

[9] D. Easley and J. Kleinberg, Strong and weak ties, in *Networks, Crowds, and Markets: Reasoning About a Highly Connected World* (Cambridge University Press, Cambridge, 2010), p. 47.

[10] M. Granovetter, Threshold models of collective behavior, Am. J. Sociol. **83**, 1420 (1978).

[11] T. C. Schelling, Dynamic models of segregation, J. Math. Sociol. **1**, 143 (1971).

[12] M. Karsai, N. Perra, and A. Vespignani, Time varying networks and the weakness of strong ties, Sci. Rep. **4**, 4001 (2014).

[13] J. P. Gleeson, Binary-state dynamics on complex networks: Pair approximation and beyond, Phys. Rev. X **3**, 021004 (2013).

[14] D. J. Daley and D. G. Kendall, Stochastic rumours, IMA J. Appl. Math. **1**, 42 (1965).

[15] D. P. Maki, *Mathematical Models and Applications: With Emphasis on the Social, Life, and Management Sciences* (Pearson College Division, Upper Saddle River, NJ, 1973).

[16] M. Barthélemy, A. Barrat, R. Pastor-Satorras, and A. Vespignani, Velocity and hierarchical spread of epidemic outbreaks in scale-free networks, Phys. Rev. Lett. **92**, 178701 (2004).

[17] R. Pastor-Satorras, C. Castellano, P. Van Mieghem, and A. Vespignani, Epidemic processes in complex networks, Rev. Mod. Phys. **87**, 925 (2015).

[18] D. Centola and M. Macy, Complex contagions and the weakness of long ties, Am. J. Sociol. **113**, 702 (2007).

[19] D. J. Watts, A simple model of global cascades on random networks, Proc. Natl. Acad. Sci. USA **99**, 5766 (2002).

[20] A. Barrat, M. Barthelemy, and A. Vespignani, *Dynamical Processes on Complex Networks* (Cambridge university press, Cambridge, 2008).

[21] W. Chen, C. Castillo, and L. V. Lakshmanan, *Information and Influence Propagation in Social Networks* (Springer Nature, London, 2022).

[22] Y. Moreno, M. Nekovee, and A. F. Pacheco, Dynamics of rumor spreading in complex networks, Phys. Rev. E **69**, 066130 (2004).

[23] D. Centola, The spread of behavior in an online social network experiment, Science **329**, 1194 (2010).

[24] M. S. Granovetter, The strength of weak ties, Am. J. Sociol. **78**, 1360 (1973).

[25] Z. Yang and T. Zhou, Epidemic spreading in weighted networks: An edge-based mean-field solution, Phys. Rev. E **85**, 056106 (2012).

[26] S. Unicomb, G. Iñiguez, and M. Karsai, Threshold driven contagion on weighted networks, Sci. Rep. **8**, 3094 (2018).

[27] M. De Domenico, C. Granell, M. A. Porter, and A. Arenas, The physics of spreading processes in multilayer networks, Nat. Phys. **12**, 901 (2016).

[28] S. Unicomb, G. Iñiguez, J. Kertész, and M. Karsai, Reentrant phase transitions in threshold driven contagion on multiplex networks, Phys. Rev. E **100**, 040301 (2019).

[29] P. Holme and F. Liljeros, Birth and death of links control disease spreading in empirical contact networks, Sci. Rep. **4**, 4999 (2014).

[30] M. Karsai, M. Kivelä, R. K. Pan, K. Kaski, J. Kertész, A.-L. Barabási, and J. Saramäki, Small but slow world: How network topology and burstiness slow down spreading, Phys. Rev. E **83**, 025102 (2011).

[31] M. Karsai, G. Iñiguez, R. Kikas, K. Kaski, and J. Kertész, Local cascades induced global contagion: How heterogeneous thresholds, exogenous effects, and unconcerned behaviour govern online adoption spreading, Sci. Rep. **6**, 27178 (2016).

[32] A. Badie-Modiri, A. K. Rizi, M. Karsai, and M. Kivelä, Directed percolation in temporal networks, Phys. Rev. Res. **4**, L022047 (2022).

[33] M. Kivelä, R. K. Pan, K. Kaski, J. Kertész, J. Saramäki, and M. Karsai, Multiscale analysis of spreading in a large communication network, J. Stat. Mech.: Theory Exp. (2012) P03005.

[34] S. Unicomb, G. Iñiguez, J. P. Gleeson, and M. Karsai, Dynamics of cascades on burstiness-controlled temporal networks, Nat. Commun. **12**, 133 (2021).

[35] T. Takaguchi, N. Masuda, and P. Holme, Bursty communication patterns facilitate spreading in a threshold-based epidemic dynamics, PLoS One **8**, e68629 (2013).

[36] F. Karimi and P. Holme, Threshold model of cascades in empirical temporal networks, Physica A **392**, 3476 (2013).

[37] M. Karsai, H.-H. Jo, and K. Kaski, *Bursty Human Dynamics* (Springer, Berlin, 2018).

[38] G. Cencetti, D. A. Contreras, M. Mancastroppa, and A. Barrat, Distinguishing simple and complex contagion processes on networks, Phys. Rev. Lett. **130**, 247401 (2023).

[39] D. A. Contreras, G. Cencetti, and A. Barrat, Infection patterns in simple and complex contagion processes on networks, PLoS Comput. Biol. **20**, e1012206 (2024).

[40] E. Andres, G. Ódor, I. Iacopini, and M. Karsai, Distinguishing mechanisms of social contagion from local network view, npj Complex. **2**, 8 (2025).

[41] L. Hébert-Dufresne, S. V. Scarpino, and J.-G. Young, Macroscopic patterns of interacting contagions are indistinguishable from social reinforcement, Nat. Phys. **16**, 426 (2020).

[42] A. Czaplicka, R. Toral, and M. San Miguel, Competition of simple and complex adoption on interdependent networks, Phys. Rev. E **94**, 062301 (2016).

[43] F. Diaz-Diaz, M. San Miguel, and S. Meloni, Echo chambers and information transmission biases in homophilic and heterophilic networks, Sci. Rep. **12**, 9350 (2022).

[44] P. D. Karampourniotis, S. Sreenivasan, B. K. Szymanski, and G. Korniss, The impact of heterogeneous thresholds on social contagion with multiple initiators, PLoS One **10**, e0143020 (2015).

[45] P. S. Dodds and D. J. Watts, Universal behavior in a generalized model of contagion, Phys. Rev. Lett. **92**, 218701 (2004).

[46] W. Wang, M. Tang, P. Shu, and Z. Wang, Dynamics of social contagions with heterogeneous adoption thresholds: crossover phenomena in phase transition, New J. Phys. **18**, 013029 (2016).

[47] B. Min and M. San Miguel, Competing contagion processes: Complex contagion triggered by simple contagion, Sci. Rep. **8**, 10422 (2018).

[48] N. Horsevad, D. Mateo, R. E. Kooij, A. Barrat, and R. Bouffanais, Transition from simple to complex contagion in collective decision-making, Nat. Commun. **13**, 1442 (2022).

[49] N. Perra, B. Gonçalves, R. Pastor-Satorras, and A. Vespignani, Activity driven modeling of time varying networks, Sci. Rep. **2**, 469 (2012).

[50] M. Starnini and R. Pastor-Satorras, Topological properties of a time-integrated activity-driven network, Phys. Rev. E **87**, 062807 (2013).

[51] Here we define the activity as an activation probability. Other works [50] consider a_i as an activation rate, or probability per unit time.

[52] In general the ϕ threshold is sampled from a $P(\phi)$ distribution. Here for simplicity we assume that $P(\phi)$ is a dirac distribution; thus each node has the same adoption threshold.

[53] M. E. Newman, The structure and function of complex networks, SIAM Rev. **45**, 167 (2003).

[54] A. Moinet, M. Starnini, and R. Pastor-Satorras, Burstiness and aging in social temporal networks, Phys. Rev. Lett. **114**, 108701 (2015).

[55] M. Abramowitz and I. A. Stegun, *Handbook of Mathematical Functions* (Dover, New York, 1972).